SRB-2: a promiscuous rainbow aptamer for live-cell RNA imaging

Murat Sunbul and Andres Jäschke [ORCID]*

Institute of Pharmacy and Molecular Biotechnology, Heidelberg University, Im Neuenheimer Feld 364, Heidelberg, 69120, Germany

ABSTRACT

The SRB-2 aptamer originally selected against sulforhodamine B is shown here to promiscuously bind to various dyes with different colors. Binding of SRB-2 to these dyes results in either fluorescence increase or decrease, making them attractive for fluorescence microscopy and biological assays. By systematically varying fluorophore structural elements and measuring dissociation constants, the principles of fluorophore recognition by SRB-2 were analyzed. The obtained structure-activity relationships allowed us to rationally design a novel, bright, orange fluorescent turn-on probe (TMR-DN) with low background fluorescence, enabling no-wash live-cell RNA imaging. This new probe improved the signal-to-background ratio of fluorescence images by one order of magnitude over best previously known probe for this aptamer. The utility of TMR-DN is demonstrated by imaging ribosomal and messenger RNAs, allowing the observation of distinct localization patterns in bacteria and mammalian cells. The SRB-2 / TMR-DN system is found to be orthogonal to the Spinach/DFHBI and MG/Malachite green aptamer/dye systems.

INTRODUCTION

Methods for the real-time visualization of RNA in single cells are indispensable to reveal their function, localization, processing and dynamics [1,2]. Currently the most popular approach is to use fluorescent protein (FP)-tagged RNA binding proteins (RBP), while the RNA of interest (ROI) is genetically fused to multiple repeats of the recognition motif for the RBP [3–6]. Even though tandem repeats combined with the massive protein cargo might have detrimental effects on the function of the ROI in this method, they are crucial for differentiating the fluorescence signal of the ROI from free FP-RBP and for maintaining a high signal-to-noise ratio. Other approaches to fluorescently label specific RNAs in living cells, such as microinjection [7] and complementary RNA probes [8], are either invasive or they are likely to alter RNA functions including localization, translation or degradation rate [1]. Recently, a CRISPR–Cas9 system has been tweaked to target single-stranded RNA and used for RNA imaging using Cas9–FP conjugates [9], which could make live-cell RNA imaging a straightforward and accessible practice in the near future. However, it has remained challenging to image RNAs with small-molecule fluorophores which offer significant advantages such as small size and superior fluorescence properties [10]. Post-transcriptional tRNA-modifying enzymes, tRNA^{Ile2} – agmatidine synthetase (Tias) [11] and tRNA guanine transglycosylase (TGT) [12], have been successfully used for site-specific covalent labeling of RNAs with azide, alkyne or fluorophore containing substrates. Since in this approach the fluorophores are covalently attached to the recognition motif of tRNA-modifying enzymes fused to the ROI, cells can be excessively washed after the labeling reaction to remove the background fluorescence, which results in high signal-to-background ratios. Fluorescence-enhancing RNA aptamers also hold great potential for this purpose. The ROI can be fused to a small RNA aptamer that strongly binds to a conditionally fluorescent dye, which is non-fluorescent in solution but becomes highly fluorescent when bound to the aptamer. Prominent examples of such RNA aptamers are Spinach [13], its close relatives Broccoli [14,15] and Corn [16], Mango and its derivatives [17,18], malachite green [19,20], DIR2s [21,22], BHQ [23,24] and SRB-2 [25–28], which have been successfully employed for imaging highly abundant and stable RNAs in live or fixed cells. Here, we investigated the substrate promiscuity of the SRB-2 aptamer in detail and discovered a panel of different-colored, very bright fluorescence turn-on dyes which were previously unknown to be SRB-2 ligands. These fluorogenic dyes allowed us to image mRNAs and rRNAs with distinct localization patterns in living bacterial and mammalian cells.

MATERIALS AND METHODS

General materials and methods

All reagents were purchased from Sigma-Aldrich or Thermo Fisher Scientific unless otherwise specified

*To whom correspondence should be addressed. Tel: +49 6221 544851; Fax: +49 6221 546430; Email: jaeschke@uni-hd.de

and used without further purification. Reverse phase HPLC purifications were performed on a Lobar®310-25 LiChroprep® RP-18 (40–63 μm) column (Merck) and compounds were eluted with a mixture of acetonitrile and water containing 0.1% trifluoroacetic acid. High resolution mass spectra were recorded on a Bruker microTOFQ-II ESI mass spectrometer. RNA concentrations were determined by NanoDrop ND-1000 spectrophotometer (peqLab). Fluorescence measurements were performed with a Jasco spectrofluorometer FP-6500 (Jasco). Absorbance spectra were recorded on a Cary 50 UV-Vis spectrophotometer (Varian). Agarose gels were stained with ethidium bromide and visualized by UV illumination using AlphaImager™2200. Synthetic DNA oligonucleotides were purchased from Integrated DNA Technologies (IDT). Restriction endonucleases were purchased from Thermo Fisher Scientific. HeLa cells (DSMZ, ACC 57) were cultured at 37°C under 5% CO_2 in Dulbecco's Modified Eagle's Medium, high glucose, without phenol red (Sigma Aldrich) supplemented with 10% FBS, 2 mM GlutaMAX, 100 unit/ml penicillin and 100 μg/ml streptomycin. BL21 Star™ (DE3) cells (Thermo Fisher Scientific) were typically grown at 37°C with shaking at 150 rpm in Luria-Bertani (LB) medium.

In vitro transcription of SRB-2

SRB-2 DNA sequence: 5′-GGAACCTCGCTTCGGCG ATGATGGAGAGGCGCAAGGTTAACCGCCTCAG GTTCC-3′. T7 RNA polymerase (0.2 μM) was added into a transcription mixture containing the double stranded DNA template (5′-<u>TTCTAATACGACTCACTATAGG</u> AACCTCGCTTCGGCGATGATGGAGAGGCGCA AGGTTAACCGCCTCAGGTTCC-3′, the sequence of T7 promoter is underlined, 0.5 μM), NTPs (4 mM each), DTT (10 mM), spermidine (1 mM), Tris–HCl (40 mM, pH 8.1), $MgCl_2$ (22 mM), Triton-X-100 (0.01%), BSA (40 μg/ml) and pyrophosphatase (1 U/ml). After 4 hours at 37°C, the reaction mixture was treated with DNaseI (50 U/ml) for 30 min at 37°C. RNA was purified by electrophoresis on a 10% denaturing polyacrylamide gel and excised from the gel. After soaking the gel in sodium acetate buffer (0.3 M, pH 5.2) overnight, RNA was ethanol precipitated and dissolved in water. RNA concentration was determined using NanoDrop ND-1000 Spectrophotometer and samples were stored at –20°C.

Screening for SRB-2 binders by using fluorescence spectroscopy

This screening is based on the change in fluorescence intensity or excitation/emission wavelength of fluorophores upon binding to SRB-2 aptamers. Basically, the fluorescence intensity, excitation and emission spectrum of each dye (1 μM) was recorded in the absence and presence of SRB-2 aptamer (10 μM) in a solution containing 1X buffer A (20 mM Hepes, pH 7.4, 5 mM $MgCl_2$ and 125 mM KCl) at room temperature using exactly the same fluorescence measurement settings. The molecules which showed

any change in the fluorescence features upon addition of SRB-2 aptamer were further studied in detail. Before fluorescence measurements, SRB-2 (12 μM dissolved in water) was incubated at 75°C for 2 min, and then cooled down to 25°C over 10 min to promote the correct folding of the aptamer. Then, one-fifth volume of 6× buffer A was added and the aptamer solution was incubated at 25°C for additional 10 min.

Determination of dissociation constants and turn-on/off ratios

Dissociation constants (K_d) for the SRB-2/probe complexes were determined by measuring the increase or decrease in the fluorescence intensity as a function of increasing RNA concentration in the presence of a fixed amount of the probe (10 nM for pyronin Y, pyronin B, acridine orange and TMR-DN; 50 nM for oxazine 1, Atto 495 and 9-aminoacridine) at 25°C. Just before the measurements, SRB-2 was folded in buffer A as mentioned before. First, excitation and emission spectra of the probes in 1X buffer A in the absence or presence of SRB-2 (10 μM) were recorded using the same fluorescence measurement settings. For the fluorescence turn-on probes, the excitation and emission maxima of the SRB-2/probe complex were used in the fluorescence measurement settings. On the other hand, for the fluorescence turn-off probes, the excitation and emission maxima of the probe were used in the fluorescence measurement settings. Dissociation constants were calculated after fitting the curves to the following equation by using least-square fitting (OriginPro 8.5.1):

$$F = F_0 + \frac{(F_\infty - F_0) \times \left\{ (K_D + P_0 + [Apt]) - \sqrt{([Apt] - P_0)^2 + K_D \times (K_D + 2[Apt] + 2P_0)} \right\}}{2P_0}$$

where F is the fluorescence at any given SRB-2 concentration, F_0 is the fluorescence of a free probe with an initial concentration of P_0, F_∞ is the maximum complex fluorescence, $[Apt]$ is the concentration of added SRB-2 and K_D is the dissociation constant.

The fluorescence turn-on value is defined as the ratio of the fluorescence peak intensity of the fluorophore (20 nM) in the presence of SRB-2 (the concentration should be ≥20 × K_D) to the fluorescence peak intensity of the fluorophore (20 nM) in the absence of SRB-2. For turn-on measurements and calculations, the excitation and emission maxima of the SRB-2-fluorophore complex were used. The fluorescence turn-off value is defined as the ratio of fluorescence peak intensity of the fluorophore (20 nM) in the absence of SRB-2 to the fluorescence peak intensity of the fluorophore (20 nM) in the presence of SRB-2 (the concentration of the aptamer should be ≥20 × K_D). For turn-off measurements and calculations, the excitation and emission maxima of the fluorophore were used.

Magnesium dependence of SRB-2/TMR-DN complex

The SRB-2 aptamer (1.2 μM in water) was incubated at 75°C for 2 min, and then cooled down to 25°C over 10 min

to promote the correct folding of the aptamer. Then, one-fifth volume of 6× buffer A containing different amount of magnesium ions (0–10 mM final concentration) was added and incubated for 10 min at 25°C. Fluorescence values were recorded upon addition of TMR-DN (1 μM) using the following instrument parameters: excitation wavelength of 561 nm, emission wavelength of 587 nm and slit widths of 5 nm.

Temperature dependence of SRB-2/TMR-DN complex

SRB-2 (1 μM) folded as described above in buffer A containing 1 mM of magnesium was incubated with TMR-DN (1 μM). The fluorescence decay was recorded upon increasing the temperature from 25 to 70°C using the following instrument parameters: excitation wavelength of 561 nm, emission wavelength of 587 nm, slit widths of 3 nm, temperature increase of 1°C in 2 min.

Folding assay

This assay was carried out using a slightly modified procedure of Strack *et al.* (29). SRB-2 and TMR-DN were mixed in two different ratios where either SRB-2 or TMR-DN is in excess and the fluorescence intensity of the SRB-2/TMR-DN complex was measured. First, the fluorescence intensity of a mixture containing 1 μM of SRB-2 (10-fold in excess) and 100 nM of TMR-DN was measured (F_1) where the amount of formed complex is determined by the limiting component TMR-DN. Second, the fluorescence intensity of a mixture containing 100 nM of SRB-2 and 1 μM of TMR-DN (10-fold in excess) was measured (F_2), where the amount of formed complex is determined by the limiting component SRB-2. Third, the fluorescence intensity of the 1 μM of TMR-DN was measured (F_3) for background corrections. In the first condition, we assume that there is enough correctly folded SRB-2 to complex with almost all TMR-DN. However, in the second condition, we assume that the amount of complex equals to the amount of correctly folded SRB-2. The ratio of these fluorescence intensities (after background correction for unbound excess TMR-DN) revealed the percentage of correctly folded SRB-2. Fluorescence values were measured in 20 mM Hepes (pH 7.4), 1 mM $MgCl_2$ and 125 mM KCl at 25°C and 37°C. The fraction of the correctly folded aptamer (f) was calculated by using the equation given below:

$$f = \frac{F_2 - F_3}{F_1 - 0.1 \times F_3}$$

Determination of quantum yields

For quantum yield (QY) measurements, sulforhodamine 101 (QY = 1.00 in ethanol) (30), fluorescein (QY = 0.925 in in 0.1 M sodium-borate buffer, pH 9.1) (31), oxazine 1 (QY = 0.141 in ethanol) (32) and pyronin Y (QY = 0.47 in water) (33) were used as standards. Basically, the integral of the fluorescence emission spectra and the absorbance of the substances at the excitation wavelength were measured and plotted in a graph by using at least four different concentrations of the compounds. It is important to keep the absorbance of these compounds below 0.05 to avoid inner filter effects in the fluorescence measurements. The slope of the line was compared with that of the reference compound and the quantum yields were measured by using the equation given below:

$$QY = QY_R \left(\frac{m}{m_R}\right)\left(\frac{n^2}{n_R^2}\right)$$

where m is the slope of the line obtained from the plot of the absorbance *vs.* the area under the fluorescence emission spectrum, n is the refractive index of the solvent and the subscript R refers to the reference fluorophore with a known quantum yield.

Live cell imaging of SRB-2 in *E. coli*

Imaging of SRB-2 aptamer in bacteria was performed using a slightly modified procedure of Paige (13) *et al*. BL21 Star™ (DE3) competent *E. coli* cells were transformed with either pET28-tRNA or pET28-SRB-2 plasmids. On the next day, single colonies were picked from LB-agar/Kanamycin (30 μg/ml) plates and grown in 5 mL of LB medium containing kanamycin (30 μg/ml) overnight at 37°C with shaking at 150 rpm. A fresh culture was started using the overnight culture as a starter culture with an OD_{600} of 0.05 in a 50 ml baffled Erlenmeyer flask containing 10 ml of LB medium with 30 μg/μl kanamycin. When OD_{600} was 0.4, IPTG (1 mM) was added into the flask, and cells were shaken for an additional 2–3 h at 37°C. Then, 200 μl of the culture was removed, spun down and resuspended in 1 ml of live cell imaging solution (Thermo Fisher Scientific) supplied with 5 mM $MgSO_4$. 200 μl of this suspension was transferred into a poly-D-lysine coated 8-well glass chamber and incubated at 37°C for 30 min. Finally, the wells were gently washed twice and bacteria were incubated with 500 nM of appropriate fluorogenic dye (pyronin Y, pyronin B, acridine orange, Atto 495, SR-DN or TMR-DN) in live cell imaging solution at 37°C. Bacteria were imaged after 10 min of incubation. An automated wide field epifluorescence microscope Nikon TiE equipped with a Nikon 100x Plan Apo lambda oil immersion objective (NA 1.45), a cooled CCD Hamamatsu Orca-AG camera and an on-stage TokaiHit incubator box were used for imaging. For the fluorescence illumination, a metal halide lamp and the following filter settings are used: for acridine orange and Atto 495: 470/30 nm excitation filter, 495 nm dichroic beam splitter, 525/30 nm emission filter; for TMR-DN and SR-DN: 560/40 nm excitation filter, 595 nm dichroic beam splitter, 630/60 nm emission filter. Images were analyzed by Fiji/ImageJ and the background correction was done by subtracting the mean fluorescent value of a surface area, where no *E. coli* cells are attached, from the whole image.

Live cell imaging of 5S rRNA in HeLa cells

HeLa cells were cultured at 37°C under 5% CO_2 in Dulbecco's Modified Eagle's Medium-high glucose, -without phenol red supplemented with 10% FBS, 2 mM Gluta-MAX, 100 unit/ml penicillin and 100 μg/ml streptomycin. For imaging experiments, HeLa cells were seeded overnight in μ-Slide (chambered coverslip) with 8 wells (Ibidi, ibi-Treat) to obtain 60–80% confluency. On the following day,

the cells were co-transfected with a 1:10 mixture of pcDNA-CFP (transfection control) and pAV-5S-SRB-2 using Fu-GeneHD transfection reagent (Promega) according to the manufacturer's protocol. pAV-5S plasmid was used in control experiments to observe the background fluorescence. After 24–36 h at 37°C, the medium is exchanged with FluoroBrite DMEM Media containing 2 mM GlutaMAX and 500 nM TMR-DN. HeLa cells were incubated in this serum-free medium for 30 min prior to imaging. An automated wide field epifluorescence microscope Nikon TiE equipped with a Nikon N Apo 60× lambda oil immersion objective (NA 1.40), a cooled CCD Hamamatsu Orca-AG camera and an on-stage TokaiHit incubator box were used for imaging. For the fluorescence illumination, a metal halide lamp and the following filter settings are used: for CFP: 470/30 nm excitation filter, 495 nm dichroic beam splitter, 525/30 nm emission filter; for TMR-DN: 560/40 nm excitation filter, 595 nm dichroic beam splitter, 630/60 nm emission filter. Images were analyzed by Fiji/ImageJ and the background correction was done by subtracting the mean fluorescent value of a surface area, where no HeLa cells are attached, from the whole image.

Synthesis

SR-DN and TMR-DN were synthesized and purified as described in the literature (26,27). It is worth mentioning that the synthesized dyes for *in vivo* imaging applications have to be extremely pure. Since the contact-quenched dyes are non-fluorescent, any fluorescent impurity would dramatically decrease the turn-on ratios and detrimentally affect the live cell imaging experiments.

RESULTS

Substrate promiscuity of SRB-2

The SRB-2 aptamer was originally selected against the fluorophore sulforhodamine B by SELEX (34) and binds to its target with a K_d of 310 nM (25) (Figure 1A). It was previously reported that both the xanthene ring system and the negative charges on the sulfonate groups are important for binding of the dye to the aptamer (25). Apart from that, not much was known about the structural requirements for high-affinity binding. As the recognition of negative charges by the poly-anionic RNA is a rather difficult task (35), we analyzed the structure-function relationships by measuring aptamer-target complex formation using a panel of systematically varied fluorophores (Figure 1B, Supplementary Figure S1 and S2). We first tested whether pyronin B, entirely missing the sulfonated lower aromatic ring of sulforhodamine B, could bind to SRB-2 and observed ∼1.2-fold higher affinity (K_d = 251 nM, Figure 1B), contradictory to what was reported earlier (25). Furthermore, pyronin B showed ∼7.5-fold fluorescence turn-on upon binding to SRB-2, which is an essential property for no-wash live-cell RNA imaging experiments. Based on this finding, we tested the binding affinity of SRB-2 to several other dyes with similar structures. Replacement of the two diethylamino groups on the xanthene ring of pyronin B by dimethylamine yields pyronin Y, which showed ∼4.3-fold
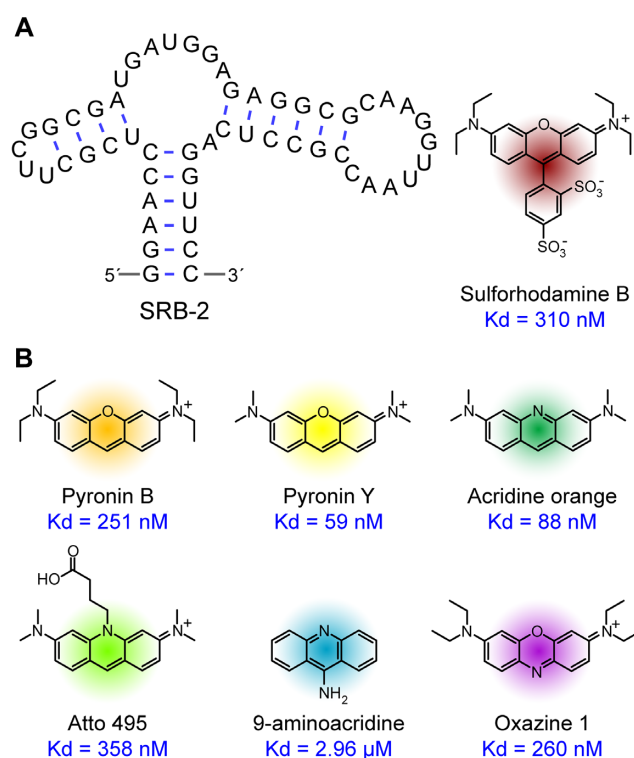
Figure 1. SRB-2 is a promiscuous RNA aptamer and can bind to many dyes with xanthene-like cores with different spectral properties. (**A**) Predicted secondary structure of SRB-2, chemical structure of its binding partner sulforhodamine B and its dissociation constant (K_d). (**B**) Chemical structures of pyronin B, pyronin Y, acridine orange, Atto 495, 9-aminoacridine and oxazine 1, and their dissociation constants (K_d) for binding the SRB-2 aptamer.

increased affinity (K_d = 59 nM) and a fluorescence turn-on of ∼4.9-fold. Fluorescence emission maxima of SRB-2-bound pyronin B or Y (578 and 575 nm, respectively) were about 20 nm blue-shifted compared to that of sulforhodamine B (596 nm) (Supplementary Figure S3). Acridine orange, which contains a nitrogen atom instead of an oxygen in the xanthene core, showed a ∼70 nm blue shift compared to sulforhodamine B, and emitted in the green region of the spectrum (emission at 525 nm) when bound to SRB-2. It presented ∼6.6-fold fluorescence turn-on upon binding to the aptamer and had only 1.5-fold lower affinity than pyronin Y towards SRB-2 (K_d = 88 nM), indicating the tolerance of the aptamer at this particular position. Even attachment of an alkyl chain to the xanthene ring nitrogen atom of acridine orange (as in Atto 495) is tolerated, reducing the affinity to roughly the value of the original target, sulforhodamine B (Figure 1B). Removal of the dimethylamino groups from the acridine orange core structure, as in the case of 9-aminoacridine, had a dramatic impact on binding affinity, reducing it 34-fold compared to acridine orange. SRB-2 was also able to bind to oxazine 1 (K_d = 260 nM), a near-IR fluorescent dye. This dye is, however, a turn-off fluorophore, as its fluorescence decreases ∼4.1-fold when bound to SRB-2, which makes it impractical for no-wash RNA imaging experiments. Considering all fluorophores tested for binding to SRB-2 (Figure 1B, Supplementary Fig-

ure S1, Table 1), we conclude that pyronin Y has the minimal structural elements required for high-affinity binding, and that SRB-2 can bind to a variety of fluorophores covering various parts of the visible and near-IR spectrum.

Imaging SRB-2 in bacteria using fluorophores with different colors

Intrigued by their high fluorescence turn-on factors and strong binding to SRB-2, we investigated the applicability of pyronin B, pyronin Y, acridine orange and Atto 495 for no-wash, live-cell RNA imaging experiments in bacteria. *E. coli* transformed with a plasmid carrying a single copy of the SRB-2 sequence embedded in a tRNA scaffold (26) were grown to OD_{600} of 0.4 at $37°C$ and the transcription was induced by addition of 1 mM IPTG. After 2 hours, bacteria were immobilized on a poly-D-lysine coated glass surface and briefly incubated with the dyes for 10 minutes at $37°C$. The fluorescence inside the SRB-2-expressing bacteria was compared to the control cells expressing only tRNA. When incubated with pyronin B, pyronin Y or acridine orange, SRB-2-expressing bacteria showed considerably higher fluorescence than the control bacteria (Figure 2A). In the case of Atto 495, we did not observe higher fluorescence, presumably due to its lower affinity towards SRB-2 and nonspecific binding to other cellular components. Pyronin Y showed the highest signal-to-background ratio (∼10-fold), calculated by the division of the average fluorescence inside the SRB-2 expressing bacteria by the fluorescence inside the control bacteria, yet acridine orange yielded a ratio of only ∼1.5-fold (Figure 2C). Although these new fluorophores increase the substrate scope and allowed for SRB-2 imaging with different colors, when compared to our previously developed fluorophore-contact quencher conjugate SR-DN (26) (Figure 2B), they exhibited significantly higher background inside the control bacteria (Supplementary Figure S4). This is likely due to known non-specific intercalation of those positively charged planar dyes into intracellular RNAs/DNAs (36), and the relatively high fluorescence quantum yields of the free fluorophores (Table 1). Thus, while not relevant for the specific binding to SRB-2, the negatively charged sulfonated aromatic ring in sulforhodamine B seems to be important for preventing unspecific DNA/RNA binding. The calculated signal-to-background ratios depend strongly on the expression level of SRB-2 in bacteria; the higher the copy number of SRB-2, the higher the signal-to-background ratio. The number of SRB-2 transcripts in this system can be controlled by changing the IPTG concentration during cell growth. We calculated the average copy number of SRB-2 per bacterium treated with 1 mM of IPTG for 2 h at $37°C$ as 3.6×10^4 (Supplementary Figure S5).

Rational design of a superior probe

The five-fold higher affinity of SRB-2 for pyronin Y, compared to its original target sulforhodamine B, made this compound a promising candidate. To reduce its background fluorescence in cells, we designed a new probe based on a commercially available 5-carboxytetramethylrhodamine fluorophore (TMR) and a dinitroaniline (DN) contact quencher. The new probe, named TMR-DN, introduces three critical features (Figure 2D): A pyronine Y core for high fluorescence, a negatively charged carboxylate-functionalized aromatic ring which should – similar to the sulfonated ring in sulforhodamine B – reduce non-specific binding to genomic DNA or RNA, and a tethered dinitroaniline moiety for inducing formation of a non-fluorescent intramolecular ground state dimer (26) between the fluorophore and dinitroaniline in the absence of SRB-2, as previously demonstrated for sulforhodamine B. Ideally, the contact quenching in TMR-DN would be completely abolished in the presence of SRB-2, resulting in a dramatic fluorescence increase. TMR-DN was found to not only retain the high binding affinity of pyronine Y to SRB-2 ($K_d = 35$ nM), but also displayed a fluorescence turn-on factor of ∼17-fold (Figure 2E). In addition, the fluorescence of TMR-DN did not change significantly in the presence of total RNA (Figure 2e), indicating low nonspecific interactions *in vitro*. Furthermore, TMR-DN demonstrated much lower non-specific background fluorescence in live bacteria than pyronin B and pyronin Y (Supplementary Figure S4) *in vivo*, and showed 49-, 27- and 9-fold higher signal-to-background ratio in SRB-2-expressing bacteria compared to pyronin B, pyronin Y and SR-DN, respectively (Figure 2C). Finally, the excitation and emission maxima of the complex were measured to be 561 and 587 nm, respectively (Supplementary Figure S6), lying in the orange region of the spectrum where the cellular auto-fluorescence is low.

Direct comparison between SR-DN and TMR-DN

SR-DN was previously developed to image SRB-2 aptamer in live cells (26). Its fluorescence increases ∼105-fold upon binding to SRB-2 displaying a high fluorescence turn-on ratio; but it has a rather low affinity to SRB-2 ($K_d = 1.3$ μM). Here, we rationally designed a new probe (TMR-DN) with a high affinity to SRB-2 ($K_d = 35$ nM), ∼38-fold better than that of SR-DN. On the other hand, the fluorescence turn-on ratio was found to be 17-fold, which is ∼6-fold lower than that of SR-DN. Therefore, it is not obvious to anticipate which probe would result in better fluorescence signal *in vivo*. In Figure 2, the signal-to-background ratios for each individual probe were compared by calculating the ratio of the average fluorescence inside the SRB-2-expressing bacteria to the fluorescence intensity inside the control bacteria. Although the control bacteria and the SRB-2 expressing bacteria were imaged under the same conditions for each dye, a direct comparison between SR-DN or TMR-DN fluorescence intensity in SRB-2 expressing bacteria cannot be made in this experiment due to different exposure times and different contrast settings. Therefore, in Figure 3 SRB-2 expressing and control bacteria (treated with 1 mM IPTG) incubated with 250 nM of either SR-DN or TMR-DN were imaged using exactly the same exposure times and the bacterial images are shown using exactly the same contrast settings. For both probes, SRB-2 expressing bacteria displayed significantly higher fluorescence than the control bacteria. Similar to the results obtained with signal-to-background ratios (Figure 2C), TMR-DN has proven to be a superior probe: SRB-2 expressing bacteria incubated with TMR-DN

Table 1. Photophysical and binding properties of different fluorophores in the presence or absence of SRB-2 aptamer

Fluorophore	λ_{max} (nm)	λ_{em} (nm)	ε ($M^{-1}cm^{-1}$)	Fluorescence Change[a]	K_d (nM)	QY	Relative Brightness[b]
9-Aminoacridine	401	456	ND	-	-	ND[c]	ND
9-Aminoacridine + SRB-2	400	455	ND	4.5-fold OFF	2960±240	ND	ND
Atto 495	498	524	88 800	-	-	0.20	56
Atto 495 + SRB-2	509	526	87 400	11.9-fold ON	358±10	0.98	270
Acridine orange	485	528	60 000	-	-	0.25	47
Acridine orange + SRB-2	498	523	58 400	6.6-fold ON	88±8	0.84	155
Pyronin B	553	570	110 600	-	-	0.39	136
Pyronin B + SRB-2	559	576	110 400	7.5-fold ON	251±50	0.90	312
Pyronin Y	557	565	101 300	-	-	0.47	149
Pyronin Y + SRB-2	559	575	106 200	4.9-fold ON	59±9	0.94	314
TMR-DN	557	579	64 000	-	-	0.027	5
TMR-DN + SRB-2	564	587	90 500	17-fold ON	35±1	0.33	94
SR-DN[d]	574	590	46 300	-	-	0.026	4
SR-DN + SRB-2[d]	579	596	85 200	105-fold ON	1340±88	0.65	174
Oxazine 1	655	669	122 000	-	-	0.07	27
Oxazine 1 + SRB-2	669	680	111 100	4.1-fold OFF	260±21	0.03	11
EGFP[e]	489	509	53 000	-	-	0.60	100
Spinach + DFHBI[f]	469	501	24 270	1030-fold ON	537	0.72	55
DFHBI-1T + Broccoli[g]	472	507	29 600	960-fold ON	360	0.94	87
TO1-Biotin + Mango[h]	510	535	77 500	1100-fold ON	3.9	0.14	34

[a]ON represents a fluorescence increase after binding to SRB-2, and OFF represents a fluorescence decrease after binding to SRB-2.
[b]Brightness is reported relative to EGFP.
[c]ND indicates not determined.
[d]Values obtained from reference (26).
[e]Values obtained from reference (45).
[f]Values obtained from reference (13).
[g]Values obtained from reference (46).
[h]Values obtained from reference (17).

displayed ∼11-fold higher fluorescence intensity than those incubated with SR-DN (Figure 3).

Next, a biologically more relevant comparison was made at lower expression levels of SRB-2, using different concentrations of SR-DN and TMR-DN. This time, bacteria transformed with either SRB-2 or tRNA plasmid were grown in the absence of IPTG. When no IPTG is present, bacteria transcribe lower amounts of SRB-2 due to the basal expression of a small amount of T7 RNA polymerase under the control of lac *operator*. The average copy number of SRB-2 per bacterium was determined as 9.4×10^2, which is ∼38-fold less than the average copy number measured at 1 mM IPTG (3.6×10^4, Supplementary Figure S5). SRB-2 expressing and control bacteria grown without IPTG were incubated with different concentrations of SR-DN or TMR-DN (2 μM, 1 μM, 500 nM, 250 nM) and subsequently imaged (Figure 4). At 2 μM, both probes resulted in extremely high fluorescence in control and SRB-2 expressing bacteria, making it impossible to distinguish the SRB-2 fluorescence from the non-specific background fluorescence. Lower concentrations of SR-DN (1 μM, 500 nM and 250 nM) reduced the background fluorescence in the control bacteria; however, the fluorescence signal inside the SRB-2 expressing bacteria decreased to a similar level. Consequently, imaging of SRB-2 at these reduced expression levels was not possible with SR-DN. In contrast, the fluorescence intensity inside the SRB-2 expressing cells was always significantly higher than that of the control cells when 1 μM or less TMR-DN was used. Signal-to-background ratios of ∼2.9, ∼3.6 and ∼11.2 were obtained with 1 μM, 500 nM and 250 nM TMR-DN, respectively. This experiment demonstrates that TMR-DN is noticeably more sensitive than SR-DN probe for imaging less abundant RNAs.

Characterization of the SRB-2/TMR-DN complex

Next, we explored the biophysical properties of the complex between TMR-DN and SRB-2. The fluorescence intensity of the complex was found to decrease from 25 to 70°C (Figure 5A), and the half-point of this transition was calculated to be 41.3 ± 0.3°C, demonstrating that >60% of the initial fluorescence signal is retained when imaging at 37°C. Subsequently, the percentage of correctly folded SRB-2 capable of binding to TMR-DN was determined (29) to be 67 ± 4% and 63 ± 3% at 25 and 37°C, respectively (Supplementary Figure S7), indicating that the change in quantum yield, rather than aptamer unfolding, is mainly responsible for the fluorescence decrease with increasing temperature.

The dependence of the fluorescence intensity on the magnesium ion concentration, which is generally between ∼0.25 and 1 mM in cells depending on the tissue type and physiological state (37), was also studied. No significant change in the fluorescence intensity of the complex was observed between 0.5 and 10 mM magnesium ion concentration. More than 80% of the fluorescence was retained even at 0.25 mM Mg^{2+} (Figure 5B), indicating that the aptamer–probe combination works at physiological Mg^{2+} concentrations.

Live-cell imaging of rRNA and mRNA

Following the characterization of the SRB-2/TMR-DN complex, we demonstrated the utility of this system by
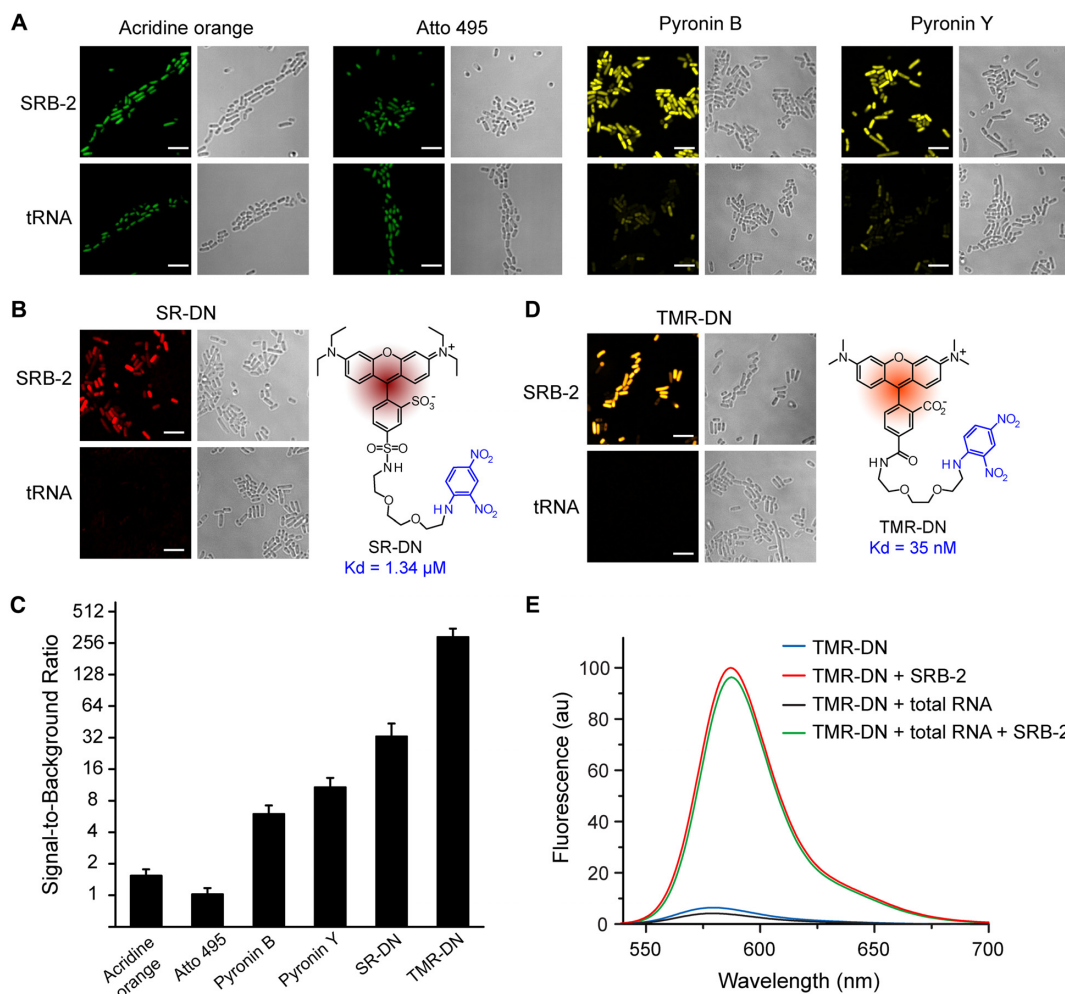
Figure 2. Live-cell imaging of the SRB-2 aptamer in bacteria using a variety of fluorophores. (**A**) Bacteria were transformed with a plasmid carrying either one copy of SRB-2 embedded in a tRNA scaffold or only tRNA and then incubated with 500 nM of acridine orange, Atto 495, pyronin B or pyronin Y. (**B**) The chemical structure of SR-DN and imaging of SRB-2 with SR-DN (500 nM) as described in (A). (**C**) Signal-to-background ratios of various fluorophores in bacteria. For no-wash live-cell RNA imaging experiments, the signal-to-background ratio was calculated by taking the ratio of the average fluorescence inside the SRB-2-expressing bacteria to the fluorescence intensity inside the control bacteria in the presence of the probes. The data represent the mean of two independent experiments; in each experiment more than 40 bacteria were analyzed. Error bars indicate standard deviation. (**D**) The chemical structure of TMR-DN and imaging of SRB-2 with TMR-DN (500 nM) as described in (A). Scale bars, 5 μm. (**E**) Fluorescence emission spectra of TMR-DN (100 nM) alone (blue), in the presence of SRB-2 (500 nM, ~10 μg/ml, red), in the presence of total RNA (0.5 mg/ml, black), and in the presence of both SRB-2 and total RNA (green). The fluorescence peak intensity of TMR-DN increases 17-fold in the presence of SRB-2.
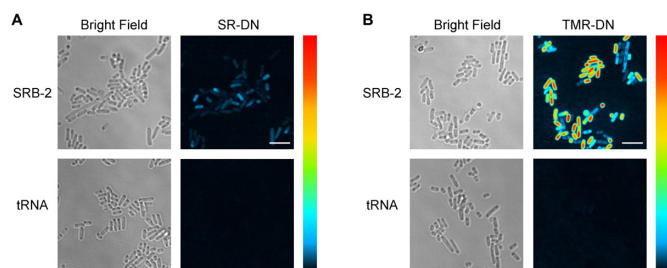

Figure 3. Direct comparison between SR-DN and TMR-DN probes at high expression levels. Bacteria were transformed with a plasmid carrying SRB-2 or tRNA sequences. Overexpression of SRB-2 or tRNA was achieved by addition of 1 mM IPTG. Bacteria were then incubated with 250 nM of SR-DN (**A**) or TMR-DN (**B**), and imaged using the same microscope settings. Images are shown using the same contrast. Scale bars, 5 μm.

imaging several different RNAs in live cells. First, the system was applied to image 5S rRNA, a rather stable and abundant RNA, in mammalian cells using a single repeat of SRB-2 embedded in a tRNA scaffold. The nuclear and cytoplasmic distribution of 5S rRNA (13,38) could be clearly visualized using a 5S-SRB-2 construct in HeLa cells, whereas control cells transfected with a plasmid carrying the 5S rRNA without SRB-2 tag showed minimal background fluorescence (Figure 6A). Next, mRNAs were imaged in live prokaryotic and eukaryotic cells, which is more challenging due to their lower abundance, shorter half-life and varying structures. To this end, 6 and 15 tandem repeats of SRB-2 (without tRNA scaffold) were fused to the 3′-UTR of GFP mRNA to amplify the signal. Bacteria expressing GFP-6xSRB-2 and GFP-15xSRB-2 demonstrated significantly higher fluorescence in the TMR channel than the bacteria expressing only GFP after incubation with TMR-DN
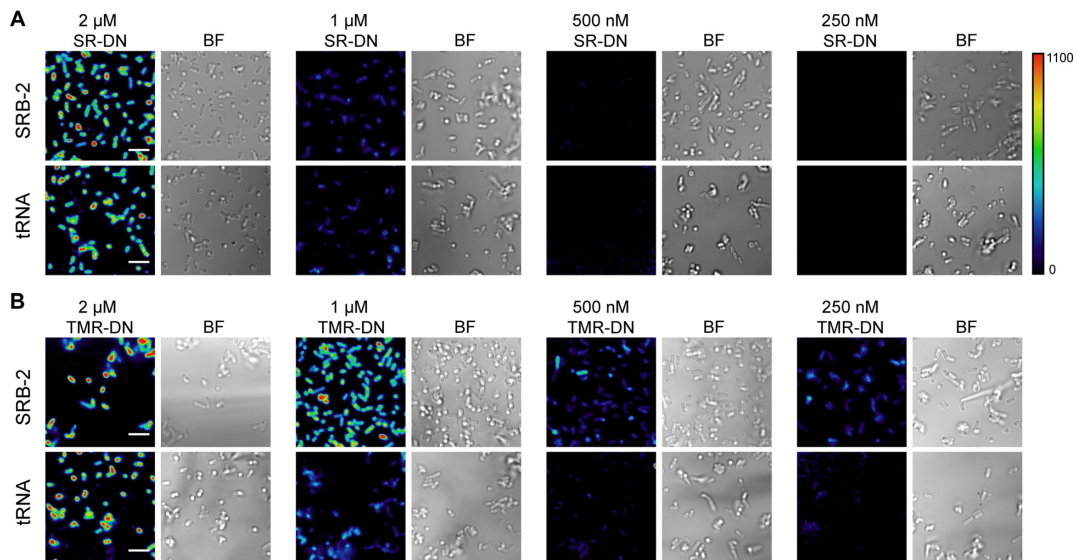
Figure 4. Direct comparison between SR-DN and TMR-DN probes at lower expression levels. Bacteria were transformed with a plasmid carrying SRB-2 or tRNA sequences and grown in the absence of IPTG to keep the copy number of SRB-2 low. Bacteria were then incubated with varying concentrations (2 μM, 1 μM, 500 nM, 250 nM) of SR-DN (**A**) or TMR-DN (**B**), and imaged using the same microscope settings. Images are shown using the same contrast. Scale bars, 5 μm.
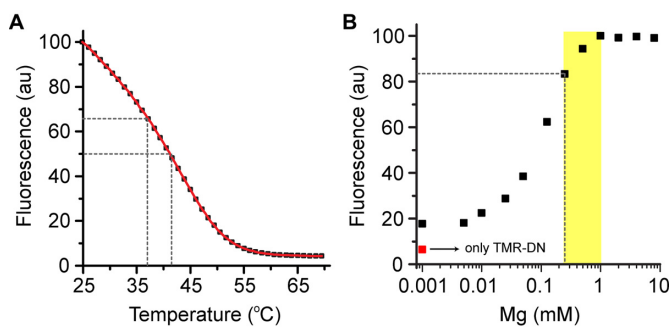
Figure 5. Properties of the SRB-2/TMR-DN complex. (**A**) Temperature dependence of the fluorescence intensity of the SRB-2/TMR-DN complex. The fluorescence decreased to 67% and 50% of the initial value at $37.0 \pm 0.3°C$ and $41.3 \pm 0.3°C$, respectively. (**B**) Dependence of the complex fluorescence on magnesium ion concentration. The fluorescence intensity of the complex in the presence of 0.25 mM magnesium is 83% of that of the complex in the presence of 1 mM magnesium. The yellow region designates the physiologically relevant concentration range of magnesium. The red square indicates the fluorescence of the TMR-DN in the absence of SRB-2 and magnesium.

(Figure 6B). We observed accumulation of GFP mRNA at the poles of bacteria, likely due to the localization of the pET plasmids at the poles (39,40), where GFP mRNAs are transcribed from the DNA template. As expected, bacteria carrying 15 repeats of SRB-2 are ~2.4-fold brighter than the bacteria carrying 6 repeats (Figure 6B). The similar levels of GFP fluorescence in bacteria transfected with different plasmids (pET-GFP, pET-GFP-6xSRB-2 or pET-GFP-15xSRB-2) imply that the addition of SRB-2 tandem repeats to GFP mRNA does not significantly affect translation efficiency. Finally, we imaged mRNAs in mammalian cells, and 15 repeats (without tRNA scaffold) of SRB-2 were fused to the 3′-UTR of CFP-TM (cyan fluorescent protein with N-terminal secretion signal and the

C-terminal transmembrane anchoring domain of platelet-derived growth factor receptor). HeLa cells were transfected with either CFP-TM (control) or CFP-TM-15xSRB-2 plasmids, and membrane localization of the CFP in the transfected cells was observed. Cells transfected with CFP-TM-15xSRB-2 displayed significantly higher fluorescence in the TMR channel than the control cells with mostly cytoplasmic distribution of the mRNAs (Figure 6C).

DISCUSSION

Here, we demonstrated the utility of the genetically encoded SRB-2 tag for imaging several different RNAs with different localization patterns in bacteria and mammalian cells. An important discovery in this study is the identification of TMR-DN as a high-affinity binder of the SRB-2 aptamer, presenting a 38-fold improvement in binding affinity, and improved signal-to-background ratios in images compared to the previously reported SR-DN probe (Figures 3 and 4). TMR-DN shows low background fluorescence in cells, and its fluorescence increases about 17-fold upon binding to SRB-2. These features allowed no-wash mRNA imaging in living cells with TMR-DN, which was not possible with SR-DN. As can be seen from Figure 4, TMR-DN was also used to image SRB-2 expressed at lower levels, where SR-DN did not work at all. In this experiment, despite the fact that SRB-2 was expressed at basal levels in the absence of IPTG, each bacterium still contains around ~900 copies of SRB-2. To image truly rare RNAs or to increase signal-to-background ratios, tandem repeats of SRB-2 can be utilized. Particularly, RNA imaging in mammalian cells is more challenging due to lower expression levels of RNAs, a more complex transcriptome and higher cellular autofluorescence (41). Therefore, tandem repeats of fluorogenic aptamers can be of great help for imaging less stable and low abundant RNAs. However, tandem repeats come with a
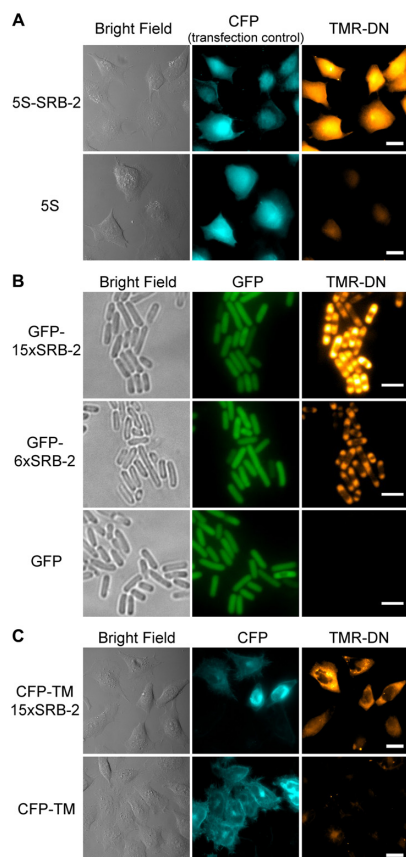
Figure 6. No-wash live-cell imaging of different types of RNAs in bacterial and mammalian cells. (**A**) HeLa cells were cotransfected with a plasmid transcribing 5S-SRB-2 under the control of the original 5S promoter and a plasmid expressing cytoplasmic CFP (transfection control) to distinguish transfected from untransfected cells. In the control (lower panel) a plasmid containing the 5S rRNA sequence (without SRB-2) was used. Cells were incubated with 500 nM of TMR-DN and then images were taken. Scale bars, 20 μm. (**B**) Imaging of GFP mRNA in bacteria. *E. coli* were transformed with a plasmid carrying GFP (control) or GFP-15xSRB-2 or GFP-6xSRB-2. After induction of the GFP expression, bacteria were incubated with 500 nM of TMR-DN and the images were taken. Scale bars, 5 μm. (**C**) Imaging of CFP-TM mRNA in mammalian cells. HeLa cells were transfected with a plasmid carrying CFP-TM (control) or CFP-TM-15xSRB-2. 24–36 hours after transfection, cells were incubated with 500 nM of TMR-DN and then images were taken. Scale bars, 20 μm.

price: they significantly increase the size of ROI, and they might alter the function and stability of ROI. For example, it was reported that certain mRNAs fused to tandem repeats of the MS2-binding RNA motif cannot be completely degraded by XRN1, the major eukaryotic 5′-3′ exoribonuclease involved in mRNA decay, due to stable interaction between MS2-GFP and the MS2-binding RNA motif (42). This caused accumulation of 3′ mRNA fragments (MS2 tandem repeats without ROI sequence) in the cells, making it very difficult to determine whether the fluorescence signal is coming from the full-length transcript or from the 3′ fragments. To investigate whether we face the same problems with SRB-2 tandem repeats, we isolated total RNA from HeLa cells transfected with plasmid pDisplay-CFP-TM-15xSRB-2 and grown in the presence of TMR-DN. Northern blot analysis using radioactive probes against SRB-2

showed a single major band matching the size of full-length CFP-TM-15xSRB-2 mRNA (Supplementary Figure S8). Accordingly, we conclude that the fluorescence signal in the TMR channel in Figure 6C was not caused by 3′ decay products, but indeed originated from the full-length transcript. In principle, this experiment has to be performed and analyzed for every RNA to be imaged with tandem repeats.

Though TMR-DN showed the best signal-to-background ratios, it is possible to use fluorogenic pyronin Y, pyronin B or SR-DN with distinct fluorescence properties for imaging of highly abundant RNAs in bacteria. However, for imaging experiments in mammalian cells, TMR-DN is the best choice owing to its low background, high affinity to SRB-2 and high turn-on ratio. The ideal concentration of TMR-DN for SRB-2 imaging depends on the expression level of the ROI and has to be optimized to obtain the highest signal-to-background ratio in cells.

We also found that SRB-2 is completely orthogonal to Spinach/Broccoli and malachite green (MG) aptamers. No cross reactivity was observed between the aptamers and their ligands (TMR-DN, malachite green and DFHBI, Supplementary Figure S9). When combined with the green fluorescent Spinach/Broccoli aptamers or far-red fluorescent MG aptamer, the orange fluorescence of the SRB-2/TMR-DN system would allow for imaging multiple RNAs. Furthermore, orthogonal fluorescent aptamer pairs provide exciting new tools for synthetic biology that could help understand the complex systems (43,44).

Another advantage of the SRB-2/TMR-DN system is its high brightness with a fluorescence quantum yield of 0.33, almost as bright as EGFP (45) (Table 1). SRB-2/TMR-DN has only two thirds of the size of EGFP and is disturbed to a smaller extent by autofluorescence compared to other green fluorescent proteins or aptamers (41). While already suitable for imaging abundant RNAs in both prokaryotes and eukaryotes, further improvements in this system will allow imaging rare RNAs with smaller repeat numbers of SRB-2, likely resulting in minimized perturbations of the RNA's function.

SUPPLEMENTARY DATA

Supplementary Data are available at NAR Online.

REFERENCES

1. Tyagi,S. (2009) Imaging intracellular RNA distribution and dynamics in living cells. *Nat. Methods*, **6**, 331–338.
2. Rau,K. and Rentmeister,A. (2017) Making the message clear: concepts for mRNA imaging. *ACS Cent. Sci.*, **3**, 701–707.

3. Hocine,S., Raymond,P., Zenklusen,D., Chao,J.A. and Singer,R.H. (2013) Single-molecule analysis of gene expression using two-color RNA labeling in live yeast. *Nat. Methods*, **10**, 119–121.

4. Daigle,N. and Ellenberg,J. (2007) LambdaN-GFP: an RNA reporter system for live-cell imaging. *Nat. Methods*, **4**, 633–636.

5. Ozawa,T., Natori,Y., Sato,M. and Umezawa,Y. (2007) Imaging dynamics of endogenous mitochondrial RNA in single living cells. *Nat. Methods*, **4**, 413–419.

6. Valencia-Burton,M., McCullough,R.M., Cantor,C.R. and Broude,N.E. (2007) RNA visualization in live bacterial cells using fluorescent protein complementation. *Nat. Methods*, **4**, 421–427.

7. Bratu,D.P., Cha,B.J., Mhlanga,M.M., Kramer,F.R. and Tyagi,S. (2003) Visualizing the distribution and transport of mRNAs in living cells. *Proc. Natl. Acad. Sci. U.S.A.*, **100**, 13308–13313.

8. Tyagi,S. and Kramer,F.R. (1996) Molecular beacons: probes that fluoresce upon hybridization. *Nat. Biotechnol.*, **14**, 303–308.

9. Nelles,D.A., Fang,M.Y., O'Connell,M.R., Xu,J.L., Markmiller,S.J., Doudna,J.A. and Yeo,G.W. (2016) Programmable RNA tracking in live cells with CRISPR/Cas9. *Cell*, **165**, 488–496.

10. Rath,A.K. and Rentmeister,A. (2015) Genetically encoded tools for RNA imaging in living cells. *Curr. Opin. Biotechnol.*, **31**, 42–49.

11. Li,F., Dong,J., Hu,X., Gong,W., Li,J., Shen,J., Tian,H. and Wang,J. (2015) A covalent approach for site-specific RNA labeling in mammalian cells. *Angew. Chem. Int. Ed. Engl.*, **54**, 4597–4602.

12. Alexander,S.C., Busby,K.N., Cole,C.M., Zhou,C.Y. and Devaraj,N.K. (2015) Site-Specific covalent labeling of RNA by enzymatic transglycosylation. *J. Am. Chem. Soc.*, **137**, 12756–12759.

13. Paige,J.S., Wu,K.Y. and Jaffrey,S.R. (2011) RNA mimics of green fluorescent protein. *Science*, **333**, 642–646.

14. Filonov,G.S., Moon,J.D., Svensen,N. and Jaffrey,S.R. (2014) Broccoli: rapid selection of an RNA mimic of green fluorescent protein by fluorescence-based selection and directed evolution. *J. Am. Chem. Soc.*, **136**, 16299–16308.

15. Filonov,G.S. and Jaffrey,S.R. (2016) RNA imaging with dimeric broccoli in live bacterial and mammalian cells. *Curr. Protoc. Chem. Biol.*, **8**, 1–28.

16. Song,W., Filonov,G.S., Kim,H., Hirsch,M., Li,X., Moon,J.D. and Jaffrey,S.R. (2017) Imaging RNA polymerase III transcription using a photostable RNA-fluorophore complex. *Nat. Chem. Biol.*, **13**, 1187–1194.

17. Dolgosheina,E.V., Jeng,S.C.Y., Panchapakesan,S.S.S., Cojocaru,R., Chen,P.S.K., Wilson,P.D., Hawkins,N., Wiggins,P.A. and Unrau,P.J. (2014) RNA mango Aptamer-Fluorophore: A bright, High-Affinity complex for RNA labeling and tracking. *ACS Chem. Biol.*, **9**, 2412–2420.

18. Autour,A., Jeng,S.C.Y., Cawte,A.D., Abdolahzadeh,A., Galli,A., Panchapakesan,S.S.S., Rueda,D., Ryckelynck,M. and Unrau,P.J. (2018) Fluorogenic RNA Mango aptamers for imaging small non-coding RNAs in mammalian cells. *Nat. Commun.*, **9**, 656.

19. Babendure,J.R., Adams,S.R. and Tsien,R.Y. (2003) Aptamers switch on fluorescence of triphenylmethane dyes. *J. Am. Chem. Soc.*, **125**, 14716–14717.

20. Yerramilli,V.S. and Kim,K.H. (2018) Labeling RNAs in live cells using malachite green aptamer scaffolds as fluorescent probes. *ACS Synth. Biol.*, **7**, 758–766.

21. Tan,X., Constantin,T.P., Sloane,K.L., Waggoner,A.S., Bruchez,M.P. and Armitage,B.A. (2017) Fluoromodules consisting of a promiscuous RNA aptamer and red or blue fluorogenic cyanine dyes: selection, characterization, and bioimaging. *J. Am. Chem. Soc.*, **139**, 9001–9009.

22. Constantin,T.P., Silva,G.L., Robertson,K.L., Hamilton,T.P., Fague,K., Waggoner,A.S. and Armitage,B.A. (2008) Synthesis of new fluorogenic cyanine dyes and incorporation into RNA fluoromodules. *Org. Lett.*, **10**, 1561–1564.

23. Murata,A., Sato,S., Kawazoe,Y. and Uesugi,M. (2011) Small-molecule fluorescent probes for specific RNA targets. *Chem. Commun. (Camb.)*, **47**, 4712–4714.

24. Sato,S.-I., Watanabe,M., Katsuda,Y., Murata,A., Wang,D.O. and Uesugi,M. (2015) Live-Cell imaging of endogenous mRNAs with a small molecule. *Angew. Chem., Int. Ed.*, **54**, 1855–1858.

25. Holeman,L.A., Robinson,S.L., Szostak,J.W. and Wilson,C. (1998) Isolation and characterization of fluorophore-binding RNA aptamers. *Fold. Des.*, **3**, 423–431.

26. Sunbul,M. and Jäschke,A. (2013) Contact-mediated quenching for RNA imaging in bacteria with a fluorophore-binding aptamer. *Angew. Chem., Int. Ed.*, **52**, 13401–13404.

27. Arora,A., Sunbul,M. and Jäschke,A. (2015) Dual-colour imaging of RNAs using quencher- and fluorophore-binding aptamers. *Nucleic Acids Res.*, **43**, e144.

28. Ying,Z.M., Wu,Z., Tu,B., Tan,W. and Jiang,J.H. (2017) Genetically encoded fluorescent RNA sensor for ratiometric imaging of microRNA in living tumor cells. *J. Am. Chem. Soc.*, **139**, 9779–9782.

29. Strack,R.L., Disney,M.D. and Jaffrey,S.R. (2013) A superfolding Spinach2 reveals the dynamic nature of trinucleotide repeat-containing RNA. *Nat. Methods*, **10**, 1219–1224.

30. Karstens,T. and Kobs,K. (1980) Rhodamine B and rhodamine 101 as reference substances for fluorescence quantum yield measurements. *J. Phys. Chem.*, **84**, 1871–1872.

31. Magde,D., Wong,R. and Seybold,P.G. (2002) Fluorescence quantum yields and their relation to lifetimes of rhodamine 6G and fluorescein in nine solvents: improved absolute standards for quantum yields. *Photochem. Photobiol.*, **75**, 327–334.

32. Rurack,K. and Spieles,M. (2011) Fluorescence quantum yields of a series of red and Near-Infrared dyes emitting at 600–1000 nm. *Anal. Chem.*, **83**, 1232–1242.

33. Bayraktutan,T., Meral,K. and Onganer,Y. (2014) Photophysical properties of pyronin dyes in reverse micelles of AOT. *J. Lumin.*, **145**, 925–929.

34. Ellington,A.D. and Szostak,J.W. (1990) In vitro selection of RNA molecules that bind specific ligands. *Nature*, **346**, 818–822.

35. Sazani,P.L., Larralde,R. and Szostak,J.W. (2004) A small aptamer with strong and specific recognition of the triphosphate of ATP. *J. Am. Chem. Soc.*, **126**, 8370–8371.

36. Shapiro,H.M. (1981) Flow cytometric estimation of DNA and RNA content in intact cells stained with Hoechst 33342 and pyronin Y. *Cytometry*, **2**, 143–150.

37. Grubbs,R.D. (2002) Intracellular magnesium and magnesium buffering. *Biometals*, **15**, 251–259.

38. Paul,C.P., Good,P.D., Li,S.X., Kleihauer,A., Rossi,J.J. and Engelke,D.R. (2003) Localized expression of small RNA inhibitors in human cells. *Mol. Ther.*, **7**, 237–247.

39. Pogliano,J., Ho,T.Q., Zhong,Z. and Helinski,D.R. (2001) Multicopy plasmids are clustered and localized in Escherichia coli. *Proc. Natl. Acad. Sci. U.S.A.*, **98**, 4486–4491.

40. Zhang,J.C., Fei,J.Y., Leslie,B.J., Han,K.Y., Kuhlman,T.E. and Ha,T. (2015) Tandem spinach array for mRNA imaging in living bacterial cells. *Sci. Rep.*, **5**, 17295.

41. Monici,M. (2005) Cell and tissue autofluorescence research and diagnostic applications. *Biotechnol. Annu. Rev.*, **11**, 227–256.

42. Garcia,J.F. and Parker,R. (2015) MS2 coat proteins bound to yeast mRNAs block 5′ to 3′ degradation and trap mRNA decay products: implications for the localization of mRNAs by MS2-MCP system. *RNA*, **21**, 1393–1395.

43. Strack,R.L., Song,W. and Jaffrey,S.R. (2014) Using Spinach-based sensors for fluorescence imaging of intracellular metabolites and proteins in living bacteria. *Nat. Protoc.*, **9**, 146–155.

44. Kellenberger,C.A., Chen,C., Whiteley,A.T., Portnoy,D.A. and Hammond,M.C. (2015) RNA-Based fluorescent biosensors for live cell imaging of second messenger cyclic di-AMP. *J. Am. Chem. Soc.*, **137**, 6432–6435.

45. Patterson,G.H., Knobel,S.M., Sharif,W.D., Kain,S.R. and Piston,D.W. (1997) Use of the green fluorescent protein and its mutants in quantitative fluorescence microscopy. *Biophys. J.*, **73**, 2782–2790.

46. Filonov,G.S., Moon,J.D., Svensen,N. and Jaffrey,S.R. (2014) Broccoli: Rapid selection of an RNA mimic of green fluorescent protein by fluorescence-based selection and directed evolution. *J. Am. Chem. Soc.*, **136**, 16299–16308.